ELSEVIER

Journal of Nuclear Materials 304 (2002) 29–49

journal of nuclear materials

www.elsevier.com/locate/jnucmat

Modelling intragranular fission gas release in irradiation of sintered LWR UO_2 fuel

Pekka Lösönen *

3, Rue des Roses, L-7249 Bereldange, Luxembourg

Received 21 May 2001; accepted 11 April 2002

Abstract

A model for the release of stable fission gases by diffusion from sintered LWR UO_2 fuel grains is presented. The model takes into account intragranular gas bubble behaviour as a function of grain radius. The bubbles are assumed to be immobile and the gas migrates to grain boundaries by diffusion of single gas atoms. The intragranular bubble population in the model at low burn-ups or temperatures consists of numerous small bubbles. The presence of the bubbles attenuates the effective gas atom diffusion coefficient. Rapid coarsening of the bubble population in increased burn-up at elevated temperatures weakens significantly the attenuation of the effective diffusion coefficient. The solution method introduced in earlier papers, locally accurate method, is enhanced to allow accurate calculation of the intragranular gas behaviour in time varying conditions without excessive computing time. Qualitatively the detailed model can predict the gas retention in the grain better than a more simple model.

PACS: 28.41.B

1. Introduction

Sintered UO_2 pellets in rods are the most common fuel type in light water reactors (LWRs). Some fission products of uranium atoms are gaseous, the most important being xenon and krypton. If the fission gases are released from the fuel matrix into the free volume of the LWR rods, increasing pressure under the cladding can finally lead to a failure of the rods. Knowledge in the fission gas release in various operating conditions is therefore necessary for determining safety margins for the fuel use. Computer simulations are required, accompanied by verifying experiments for benchmarking the models.

The gas release from sintered UO_2 fuel can take place through several mechanisms. The release by single gas atom diffusion to grain boundaries and from there to the free volume of the rod by venting through tunnels is the most important mechanism for stable gas atoms under normal operating conditions up to high burn-ups. The other release mechanisms active at low burn-ups, recoil, knock-out etc. contribute less than 1% release of the generated gas [1,2]. The release from the porous zone at the rim of the pellets starts increasing at fuel rod average cross sectional burn-ups of 40 000–50 000 MWd/tU in LWR fuel [3–6]. However, diffusion remains the mechanism having potential to much larger release fractions than the other mechanisms together even at these high doses [7].

The problem of predicting correctly the fission gas release by diffusion in LWR fuel has not been perfectly solved up till now, even though considerable experimental and theoretical work has been performed [8–10]. Modelling the release by diffusion results in a complex set of differential equations. Simplifications have been applied in physical models and in the solution methods for the equations. A widely used approach is to apply the so called effective diffusion coefficient for spherical grains and to solve the diffusion equation for time varying temperature and power histories by assuming constant conditions during the time step [11–19]. The use of the effective diffusion coefficient simply as a function of

* Tel.: +352-4301 32915.
E-mail address: pekka.loesoenen@cec.eu.int (P. Lösönen).

0022-3115/02/$ - see front matter
PII: S0022-3115(02)00856-5

temperature overlooks details like gas precipitation into and resolution from intragranular bubbles as a function of time and grain radius.

This paper concentrates on modelling the behaviour of intragranular gas in varying irradiation conditions of LWR UO_2 fuel. Only the behaviour of stable gas atoms is included. A major part of the basic model with single gas atom diffusion, precipitation into and resolution from intragranular bubbles consists of equations presented earlier by Speight, White, Tucker, Turnbull et al. [11,20]. However, new elements are introduced into the spectrum of submodels and some recent experimental findings are implemented. Further, a new solution method for the set of equations enables accurate calculation of gas precipitation into bubbles and resolution from them as a function of grain radius with a reasonable computing time. The model is described in Section 2 and the new solution method is presented in Section 3.

The effects of various model parameters on the results are examined by sensitivity analysis included in the discussion in Section 4. Example calculations show the importance of modelling the behaviour of intragranular gas accurately. A summary and conclusions are given in Section 5.

2. Model

The governing equation in spherical co-ordinates for random single gas atom diffusion in the irradiation of sintered UO_2 fuel, assuming symmetry, is

$$\frac{\partial c(r_g,t)}{\partial t} = \frac{1}{r_g^2}\frac{\partial}{\partial r_g}\left(r_g^2 D \frac{\partial c(r_g,t)}{\partial r_g}\right) + \beta(t), \tag{1}$$

where c is the gas concentration in the matrix, t the time, r_g the radial co-ordinate in the spherical grain, D the diffusion coefficient and β the gas generation rate.

The gaseous fission products xenon and krypton have a strong tendency to precipitate into bubbles in LWR oxide fuels because of their extremely low solubility. Thus, Eq. (1) is not adequate for describing the gas concentration in the solution as a function of time and grain radius. The number of gas bubbles in a unit volume of the grain, the size of the bubbles and the density of gas in them affect significantly the amount of gas atoms available for diffusion into grain boundaries.

The gas atoms diffuse into the bubbles and they can re-enter into the UO_2 lattice from the bubbles by means of thermal resolution or by irradiation resolution. In this work the thermal resolution is ignored, since there is no direct evidence that it exists for gas in intragranular fission gas bubbles in UO_2 fuel [21–23]. The rate of the change of the amount of gas in intragranular bubbles, $m(r_g,t)$ (mol/cm^3), is

$$\frac{dm(r_g,t)}{dt} = g_b(r_g,t)C_b(r_g,t) - j_{ri}(r_g,t), \tag{2}$$

where g_b is the capture rate of a bubble with an average radius (mol/s), C_b the density of the bubbles (cm^{-3}) and j_{ri} the resolution rate from the bubbles back into the UO_2 matrix due to irradiation effects (mol/cm^3 s).

The modelling of various terms in Eqs. (1) and (2) is explained below.

2.1. Diffusion coefficient, D

The diffusion coefficient is a function of at least temperature, fission rate, burn-up and stoichiometry [24–26]. At very low burn-ups, 1–10 MWd/tU, the xenon diffusion coefficient in UO_2 decreases significantly [27]. This is most probably due to the establishment of radiation damage in the matrix forming traps for the gas atoms. After the decrease at very low burn-ups, the diffusion coefficient does not change as a function of burn-up at constant temperature, although interpretations of some experimental results indicate that the xenon diffusion coefficient in UO_2 would increase with irradiation dose at high burn-ups [24].

Turnbull et al. studied carefully the xenon diffusion coefficient in irradiation of stoichiometric UO_2 fuel as a function of temperature [24,25]. They came up with an equation containing three terms:

$$D = D_1 + 4D_2 + 4D_3, \tag{3}$$

where D_1 is only temperature dependent term representing intrinsic thermal diffusion and D_2 is a function of both temperature and fission rate. D_3 is effective only close to the surface of the fuel and its contribution to the total diffusion of stable gas atoms is considered negligible. The precipitation of intragranular bubbles makes the effective diffusion coefficient smaller than the one calculated with Eq. (3).

According to Davies and Long [28], the intrinsic term is

$$D_1 = 7.6\times10^{-6}\exp\left(\frac{-70,000}{RT}\right)\ \mathrm{cm}^2/\mathrm{s}, \tag{4}$$

where R is 1.987 cal/mol K and T is temperature in K.

The second term in Eq. (3) is a rather complicated function of fission rate and temperature:

$$D_2 = s^2 j_v V,$$

$$V = \frac{\alpha_s s^2 + ZV_0}{2Z}\left[\left(1+\frac{4K'Z}{j_v(\alpha_s s^2+ZV_0)}\right)^{1/2} - 1\right],$$

$$V_0 = \exp\left(\frac{-55,200}{RT}\right), \quad j_v = 10^{13}V_0, \quad K' = KF\Omega,$$

$$s = \Omega^{1/3},$$

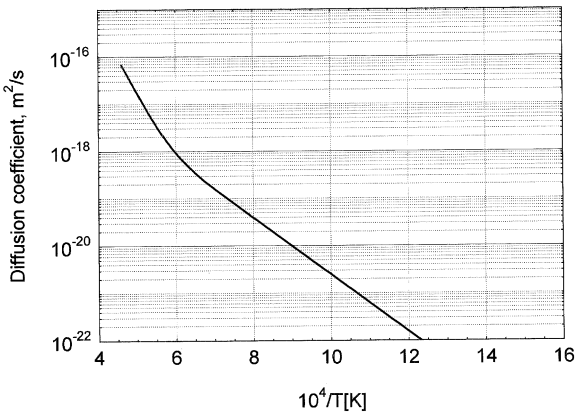

Fig. 1. Diffusion coefficient for fission gas atoms in irradiation of UO_2 [24,25].

where V is the thermodynamic vacancy concentration (vacancies/atom), α_s the fixed sink strength (10^{19} cm^{-2}), s the atomic jump distance, Ω the atomic volume, j_v the cation vacancy jump rate (s^{-1}), K' the defect production rate (s^{-1}), F the fission rate (fissions/cm^3 s), K the number of defects per fission and Z the number of sites around a point defect from which recombination is inevitable.

The purely fission rate dependent term D_3 is not taken into account, since it has no visible effect on the release of stable gas atoms.

Applying the following values for the parameters produces the diffusion coefficient as a function of temperature presented in Fig. 1:

$$Z = 100, \quad \Omega = 4.09 \times 10^{-23}\ \text{cm}^3, \quad K = 5 \times 10^5,$$

$$F = 1 \times 10^{13}\ \text{cm}^{-3}/\text{s}.$$

2.2. Capture rate, g_b

A bubble gains new gas atoms per unit time by diffusion, assuming no thermal resolution [29]

$$g_b(r_g, t) = 4\pi r D c(r_g, t), \tag{5}$$

where r is the bubble radius and c the concentration of the gas in the matrix. If the radius of the bubbles is small compared to the distance between them, Eq. (5) is valid for diffusion limited precipitation, except for a very short transient period. In normal reactor conditions the short transient period is not longer than a few tens of seconds. The component of thermal resolution would be accounted for by replacing c in Eq. (5) by the term $(c - c_0)$, where c_0 is the thermodynamic equilibrium concentration on the surface of the bubble.

2.3. Irradiation resolution rate, j_{ri}

The irradiation resolution rate, j_{ri}, is modelled to be proportional to the fission rate, F (cm^{-3}/s) [31] and to the gas concentration in the bubbles, m:

$$j_{ri}(r_g, t) = Fbm(r_g, t). \tag{6}$$

Combining (2), (5) and (6) yields the equation for the rate of the change of the gas concentration in the bubbles:

$$\frac{dm(r_g, t)}{dt} = 4\pi \bar{r}(r_g, t) D c(r_g, t) C_b(r_g, t) - Fbm(r_g, t). \tag{7}$$

The numerical value for b is defined below together with calculation of the bubble radius by using experimental data, since this information is necessary for the calculation of the amount of gas in the bubbles according to Eq. (7) in quasi-steady state conditions.

2.4. Bubble density, C_b

The sink strength of the intragranular bubble population is directly proportional to bubble density. The amount of gas in the UO_2 matrix available for diffusion into grain boundaries is therefore strongly affected by the bubble density. At low burn-ups the bubble density is only slightly temperature dependent [39]. At higher burn-ups the bubble population coarsens in elevated temperatures. A population of 100–200 nm diameter bubbles is born within 1 h in rapid transients [43]. The behaviour of the bubble density is modelled separately for low burn-up or low temperature fuel and for high burn-up – high temperature fuel, where significant coarsening is expected.

2.4.1. Low burn-up or low temperature fuel

The bubble density depends at least on temperature and burn-up. According to Baker the bubble density decreases with increasing temperature [39]. In varying conditions the kinetics of the change in the bubble density depends strongly on the irradiation effects. The intragranular bubbles are often seen in straight lines, which is interpreted to be due to bubble nucleation in the wake of energetic fission fragments [31,39]. Bubbles, at least smaller ones, can also be destroyed in irradiation, presumably by collisions with fission fragments [30]. However, there is evidence that a single collision may not always destroy the bubble, but rather distort the lattice [36]. Therefore a bubble is obviously not destroyed as a consequence of every collision.

The bubble density, C_b, as a function of temperature is modelled according to the following equation:

$$\frac{dC_b(r_g, t)}{dt} = A(T)F - 2\pi z^2 \lambda_F P F C_b(r_g, t), \tag{8}$$

where t is time, $A(T)$ the number of bubbles nucleated per fission, F the fission rate, z the radius of an effective fission spike, λ_F the fission fragment range and P the probability of a bubble to be destroyed by a fission spike. The first term on the right hand side of Eq. (8) is the birth rate and the second term the destruction rate of the bubbles. Eq. (8) resembles the one presented by Turnbull [31]. However, the birth rate of the bubbles is now temperature dependent, factor P is added, and the bubble destruction rate has no dependence on the bubble radius. It is not considered physically justified to include the dependence of the destruction rate on the small intragranular bubble radius. Although large bubbles are more often partially affected by the effective fission spike than small ones are, the probability that all the gas atoms in a large bubble would gain enough energy to be resoluted by a fission spike is low. Nelson [32] has estimated that some atoms in a bubble larger than 3 nm containing high density gas would not be completely destroyed by a single fission spike.

White and Tucker propose a birth rate for the bubbles where the first term on the right hand side of Eq. (8) is multiplied by the gas concentration in the matrix [11]. At the beginning of irradiation of fresh UO_2 a correct prediction of the bubble density could be achieved by this multiplication, but this would lead, against observations in [42], to a continuously increasing bubble density with increasing burn-up in low temperature irradiation. Therefore no dependence on the gas concentration is included. No large error is expected due to this, since the bubble population emerges already at burn-ups below 1 MWd/kgU [33–35].

The bubble nucleation rate per fission event, $A(T)$ in Eq. (8) is modelled as a function of temperature, although there is no direct evidence on this temperature dependence. However, it can be qualitatively explained: at low temperatures vacancy clusters forming the embryos of the bubbles are not healed out as quickly as at higher temperatures, thus leaving time for the embryos to stabilise and to become bubbles.

The solution for Eq. (8) is

$$C_b(t) = \frac{A(T)}{2\pi z^2 \lambda_F P}\left(1 - e^{-2\pi z^2 \lambda_F P F t}\right) + C_{b0} e^{-2\pi z^2 \lambda_F P F t}, \qquad (9)$$

where C_{b0} is the bubble density at the beginning of the time step, $t = 0$.

At steady state the following relation between $A(T)$ and P prevails:

$$\frac{A(T)}{P} = 2\pi z^2 \lambda_F C_b(T). \qquad (10)$$

Numerical values for $A(T)$ and P are found by fitting the evolution of the bubble density in time with experimental data. Results of an irradiation – annealing – irradiation experiment are reported in Ref. [36]. A new bubble population was born and the old population completely disappeared during the second irradiation up to a dose of 1.68×10^{17} fissions/cm^3 but not at 8×10^{16} fissions/cm^3. The specimens were irradiated at 1200 °C for about 2 h. The different doses were achieved by using different enrichments. The A (1200 °C) is obtained by assuming the bubble density by Baker [39], and the following values for the other parameters in Eq. (10) [37,38]:

$$\begin{aligned} &z = 3.5 \times 10^{-7} \text{ cm [37]},\\ &\lambda_F = 6 \times 10^{-4} \text{ cm [38]},\\ &P = 0.1,\ 0.05 \text{ or } 0.025. \end{aligned} \qquad (11)$$

The fission rate was 2.33×10^{13} fissions/cm^3 s. The correlation applied to the bubble density as a function of temperature in steady state was deduced by using the data in Ref. [39] as illustrated in Fig. 2:

$$C_b(T) = (15.7 - 0.00578T) \times 10^{17}, \qquad (12)$$

where T is the temperature in K.

The evolution of the calculated bubble densities by Eq. (9) as a function of time is presented in Fig. 3. It seems that a value of 0.05 for P results in a practically fully developed novel bubble population in 2 h.

The number of bubbles nucleated per fission, $A(T)$, is calculated as a function of temperature. The probability P is set to 0.05 and Eqs. (10)–(12) are employed. The results are given in Table 1.

It is interesting to see that the number of bubbles nucleated per fission by this model is about the same as that given by White and Tucker [11].

The bubble number density does not decrease only with increasing temperature, but it has also been reported to decrease with increasing burn-up. A typical bubble density of 5×10^{17} cm^{-3} at burn-ups ~10 MWd/kgU

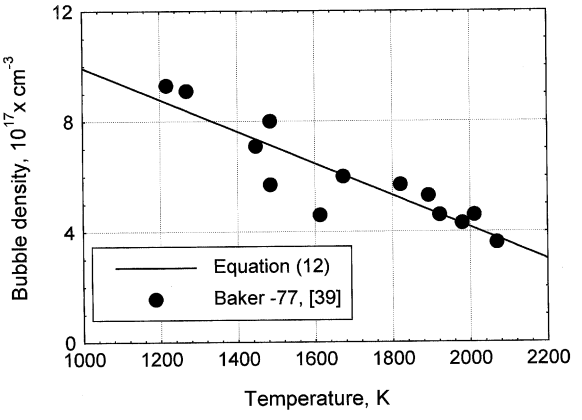

Fig. 2. Intragranular bubble density in steady state irradiation at 7.9 MWd/kgU according to measurements in [39], and by Eq. (12).

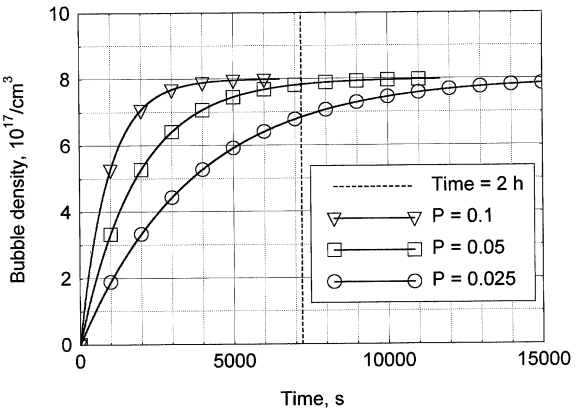

Fig. 3. Evolution of calculated bubble densities by Eq. (9) as a function of time. P is the probability for a bubble to be destroyed in a collision with an energetic fission fragment.

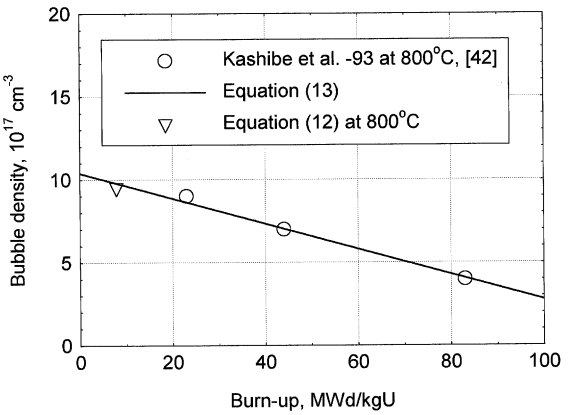

Fig. 4. The burn-up dependence of bubble density at steady state in low temperature irradiation according to measurements [39,42], and according to Eq. (13).

Table 1
Calculated number of bubbles nucleated per fission

Temperature (K)	Bubbles nucleated per fission
1273	41.6
1373	39.3
1473	36.9
1573	34.6
1673	32.3
1773	30.0
1873	27.7
1973	25.4
2073	23.1

[39], has decreased by one order of magnitude at 40 MWd/kgU according to Ray et al. [40,41]. On the other hand, Kashibe et al. interpret the small bubble density by Ray et al. to be due to enumeration of the small bubbles of ~2 nm diameter [42]. In any case, the bubble density decreases somewhat with increasing burn-up, along with the appearance of large, several tens of nanometres size bubbles at temperatures 800–1200 °C for 40–45 MWd/kgU burn-ups [40,42].

At temperatures 1300–1400 °C the population of the small bubbles disappeared from the transient tested bulk of the specimen at ~40 MWd/kgU in 48 h irradiation, but many bubbles of 4.5 nm diameter were observed in the close vicinity of large, 50–500 nm sized bubbles [40].

For the base irradiated fuel in Ref. [42] there are data up to 83 MWd/kgU. At $\leqslant 800$ °C the bubble density is in the order of 9×10^{17} cm^{-3} at 23 MWd/kgU, decreasing down to 4×10^{17} cm^{-3} at 83 MWd/kgU. The number density of the larger, 10–20 nm size bubbles increases between 44 and 83 MWd/kgU, and at the same time the total density of the bubbles decreases.

The slowly decreasing bubble density with increasing burn-up is modelled by using the experimental results by Baker [39] and by Kashibe et al. [42]. Eq. (12) is modified to include the burn-up dependence of the bubble density (Fig. 4):

$$C_b(\mathrm{BU}, T) = \frac{-0.0762\,\mathrm{BU} + 10.4}{9.8} C_b(T), \tag{13}$$

where BU is burn-up, MWd/kgU, and $C_b(T)$ is the bubble density according to Eq. (12).

2.4.2. High burn-up and high temperature fuel

Eqs. (9), (12) and (13) describe the evolution of the density of the bubble population at low burn-up, and also at higher burn-ups in low temperatures. The coarsening of the bubble population must be modelled separately. The appearance of intragranular bubbles of 100–200 nm diameter is an outstanding feature closely linked to fission gas release. The onset of the fission gas release coincides with the presence of these large bubbles [5,43]. The existence of the coarsened bubble population is seen as a dark zone in micrographs on pellet cross sections [5,43,44]. The dark area in micrographs becomes visible first in the hottest centre parts of the pellets [44,45]. At elevated temperatures or during prolonged irradiation the population of the large intragranular bubbles disappears and the dark area in the micrographs is seen as a ring or several rings indicating separate occasions of fission gas releases [5,43,45–47]. Base irradiated and ramp tested fuel may experience up to 90% local release at the centre of the pellets, and the dark ring is located in the transition zone between high release and low or zero release [43,46].

Mogensen et al. have measured intragranular swelling as a function of pellet radius for ramp tested LWR fuel rodlets [48]. The burn-up of the fuel was 35–40 MWd/kgU. The intragranular swelling occurred only at the regions where the zero release at the periphery of the pellet changed into high release in the centre of the

pellets. The maximum local swelling was 4–7%, depending on ramp characteristics. This means that almost all the gas in that region is located in the large intragranular bubbles. There is very little data in the literature about small intragranular bubbles of 2 nm diameter in the region of the dark ring. The results of Ray et al. indicate a disappearance of the small bubbles from the bulk of the fuel whenever there is a developed population of coarsened 50–300 nm bubbles [40]. It seems obvious that the density of small bubbles in coarsening decreases down to a level where the effect of this population is insignificant.

The dark rings have been observed in a wide range of burn-ups, 13–83 MWd/kgU [5,43]. The onset temperature for the coarsening depends only slightly on burn-up, at least above 50 MWd/kgU [5]. At lower burn-ups there seems to be a weak temperature dependence: coarsening starts at higher temperature at 13 MWd/kgU than at 48 MWd/kgU [43]. The reported results of Baker, and Kashibe et al. are further evidence on the burn-up dependence. Baker did not report any large bubbles at 7.9 MWd/kgU below 1700 °C, but incipient coarsening was seen in examinations of Kashibe at al. at a burn-up of 43 MWd/kgU at 800 °C [39,42]. The exact temperature where coarsening actually starts is not easy to define, since the temperature gradient is steep at the radial positions, where the dark ring is often located. Some values have been given in the literature, but there are large uncertainties involved, especially at high burn-ups where the degradation of the thermal conductivity of the fuel decreases the reliability of the estimated temperatures.

There are few data available on the kinetics of the coarsening process. Lippens reports results on ramp tests for base irradiated fuel, where the power increase was rapid and the hold time at the maximum power 1–10 min [45]. No bubble coarsening was noticed in the form of newly emerging dark areas, but the existing dark annulus in the centre of the pellets was observed to fade. Intragranular bubble coarsening has occurred in 1–4 h in some other ramp tests [43,49]. Continued irradiation at high power up to 52 h did not affect the location of the dark ring [43]. The outer borders of the dark rings are relatively sharp, but inwards the darkness often vanishes gradually. It can be concluded that the coarsening takes place in a few hours at temperatures higher than a certain threshold temperature. Furthermore, the coarsened bubbles disappear: the higher the temperature is, the faster they are lost.

The physical mechanism responsible for the obvious coarsening of the bubble population in irradiation can be attributed to bubble migration and coalescence or to Ostwald ripening. In general the former mechanism is favoured for small bubbles in irradiation and annealing [42]. For larger bubbles especially in annealing also the latter explanation is possible [42,50,51].

The mean bubble diameter $\bar{r}$ under the conditions of migration and coalescence for small bubbles with constant gas density inside them obeys the $1/6$ power in time [52]:

$$\bar{r} = \left(6\Omega^{1/3} m_{\mathrm{T}} v D_{\mathrm{s}}(p) t\right)^{1/6}, \tag{14}$$

where Ω is the atomic volume of the material (m^3), v the atomic volume of the gas in the bubbles (m^3), $D_s(p)$ the pressure dependent surface diffusion coefficient (m^2/s), t the time (s) and m_T the total gas concentration (at.%). At high temperatures the total gas concentration is close to the gas concentration in the bubbles. If the gas density in the bubbles is assumed constant, the development of the bubble density follows $t^{-1/2}$ dependence. Eq. (14) does not predict the observed change into bimodal bubble size distribution at high burn-ups or in transients. Chkuaseli and Matzke [53] have shown that a bimodal bubble size distribution can be a result of a joint action of bubble surface and volume diffusion mechanisms. They have reported results only for low burn-up annealing experiments and their calculation model is, although rather straightforward, time consuming. Evans has provided an explanation for the emergence of large bubbles in the vicinity of grain boundaries in annealing [23]. The mechanism he proposes can perhaps be applied also for the results of Chkuaseli et al. since they do not give the distribution of the coarsened bubbles as a function of grain radius.

The bubbles are proven to be almost immobile in normal LWR fuel temperatures [54–56]. No bubble migration is therefore modelled, although in very high temperatures some relaxation of the over pressure in the bubbles might trigger bubble coarsening by migration and coalescence. Ostwald ripening in a population of highly over-pressurised bubbles is not a probable coarsening mechanism. Shrinking of small over-pressurised and vacancy-starved bubbles would imply either thermal or irradiation-induced resolution of gas atoms or vacancies to the matrix. Thermal resolution of gas atoms has not been observed from fission gas bubbles in UO_2. However, irradiation resolution could serve as a mechanism for removing the gas atoms from the bubbles, thus enabling the coarsening through selective capturing of the gas atoms by bubbles of different sizes.

White [57] presented recently a model for intragranular bubble growth, which predicts reasonably well the appearance of large bubbles in annealing. The model takes into account the vacancy flow into the bubbles. Some bubbles are more favourably positioned relative to vacancy sources than the others, which are vacancy starved and do not attract new gas atoms due to a stress field around them. Ray et al. have also seen the large bubbles invariably linked to the dislocation network [40], which can possibly serve as vacancy sources. A theory of the effect of the stress field around

over-pressurised bubbles preventing them to absorb new gas atoms has been presented earlier by Ronchi [58]. However, the calculations presented by Ronchi do not answer the question of bubble size distribution. The model by White is addressed to annealing conditions and it is perhaps not directly applicable to irradiation.

Since the physical mechanism of the coarsening of intragranular bubbles in irradiation of UO_2 fuel is unknown, empirical approach is applied. The coarsening process is modelled to be triggered of at a burn-up dependent threshold temperature. Having such a threshold temperature provides the observed sharp distinction between areas where coarsening has not taken place and where the bubble population has coarsened, visible as dark zones in micrographs.

The threshold temperature in °C for the onset of the coarsening is obtained by using data in Refs. [39,42–44] (see Fig. 5):

$$T = \frac{8000}{\ln\left(\dfrac{\mathrm{BU}-9}{0.005}\right)}, \tag{15}$$

where BU is burn-up, MWd/kgU.

At 13 MWd/kgU the threshold temperature is estimated to be about 1200 °C, according to data in [43]. No coarsening is modelled below 9 MWd/kgU.

No mechanistic modelling is applied to the kinetics of the coarsening process due to the above-explained difficulties in selecting the appropriate mechanism. A simple intuitive view is to assume the speed of the change of the bubble radius to be proportional to the difference between the actual, $r(t)$, and coarsened, r_F, bubble radii:

$$\frac{\mathrm{d}r(r_g,t)}{\mathrm{d}t} = \tau\left[r(r_g,t) - r_F\right].$$

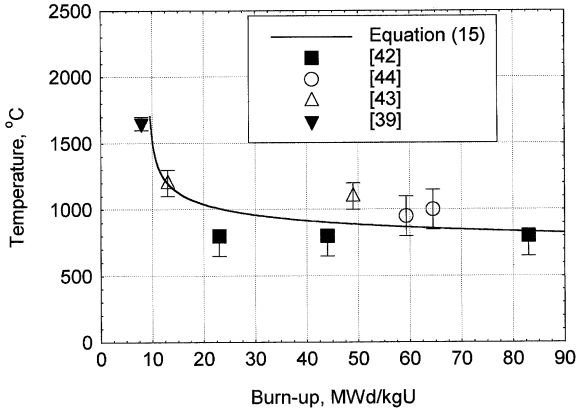

Fig. 5. Threshold temperature for intragranular bubble coarsening as a function of burn-up according to Eq. (17) and experimental data points. Solid symbols: no coarsening or only incipient coarsening; open symbols: coarsened intragranular bubble population at the end of irradiation.

Solving this equation for a time step gives the average bubble radius as a function of time:

$$r(r_g,t) = r_F\left(1 - \mathrm{e}^{-\tau\Delta t}\right) + r(r_g,t^m)\mathrm{e}^{-\tau\Delta t}, \tag{16}$$

where $r(r_g,t^m)$ is the bubble radius at the beginning of the time step, a constant and Δt the time from the beginning of the time step. The coarsened bubble radius, r_F, was selected as 100 nm. In reality the radii of coarsened bubbles vary over a wide range, from a few tens to a few hundreds of nanometers [40,59]. The effect of the choice of value of parameter r_F in Eq. (16) on fission gas release is presented in Chapter 4. Modelling accurately the kinetics of the coarsening would require a good database on measured bubble diameters in well-characterised experimental conditions. There is very little data in the literature describing the kinetics of intragranular bubble coarsening in the irradiation of UO_2 fuel. Choosing a value of 8.3×10^{-4} s^{-1} for constant τ in Eq. (16) produces a coarsened bubble population within 1 h, which is in agreement with the data in Ref. [43].

The bubble density, C_b (bubbles/cm^3) is obtained by using the bubble radius, r, and the gas concentration in the bubbles, m:

$$C_b(r_g,t) = \frac{m(r_g,t)3M}{4\pi r^3\rho}, \tag{17}$$

where ρ is the gas density in the bubbles (g/cm^3) and M the atomic mass of xenon (g/mol).

Eqs. (12), (13), (15) and (16) should be seen as an empirical and qualitative description of the development of the bubble population rather than a mechanistic physical model.

2.5. Bubble radius, r

The equation for calculating the bubble radius after the coarsening has been triggered off was given above. If no coarsening occurs, the bubble radius is calculated by using the bubble density and gas concentration in the bubbles:

$$r(r_g,t) = \left[\frac{3m(r_g,t)M}{4\pi\rho C_b}\right]^{1/3}. \tag{18}$$

Under steady state conditions a dynamic equilibrium prevails between the gas in the bubbles and in the matrix. The ratio of the amount of gas in the solution and in the bubbles can then be calculated in quasi-steady state conditions with Eq. (7):

$$\frac{c(r_g,t)}{m(r_g,t)} = \frac{Fb}{4\pi\bar{r}(r_g,t)DC_b}. \tag{19}$$

The amount of gas atoms in the matrix available for diffusion is then inversely proportional to the average intragranular bubble radius. Proper determination of

the bubble radius as a function of the amount of gas in it requires knowledge about the thermodynamic state of the gas.

Once nucleated, the embryos of the bubbles grow by gaining diffusing gas atoms and vacancies. The density of the gas in the bubbles is very high, close to solid state xenon, 2–4 g/cm^3 for larger bubbles of 10–100 nm diameter [59], and 4–6 g/cm^3 for bubbles of 4–8 nm size [60]. The pressure in the intragranular bubbles is certainly in the order of gigapascals, far above the pressure of equilibrium bubbles. The reasons for the obvious and large vacancy deficiency of the bubbles are not clear, but the irradiation can perhaps remove vacancies from the bubbles thus maintaining the over-pressure. Irradiation, more precisely the energetic fission fragments, can remove both vacancies and gas atoms from the bubbles, re-entering them back into the UO_2 matrix.

The van der Waals equation of state predicts that if xenon is in bubbles smaller than about 1 nm in mechanical equilibrium with the bulk solid surrounding them, it behaves as a constant-density condensed phase with a density of about 2.6 g/cm^3 [61]. The experimental data shows that xenon is in very high density also in larger, 4–100 nm bubbles in UO_2 irradiation [59,60]. Therefore, instead of using the van der Waals equation of state a constant bubble density of 4 g/cm^3 was chosen in Eq. (18) independent of the bubble size.

The high over-pressure might enable thermal resolution from the bubbles. Actually no direct evidence on thermal resolution from intragranular bubbles in irradiation of UO_2 is reported in the literature. Therefore no thermal resolution is accounted for in this work. Bubble growth in transients by dislocation loop punching is also a phenomenon worth considering under these conditions.

The density of the gas in the intragranular bubbles is so high that the van der Waals equation of state is not valid for evaluating the gas pressure. A better estimate on the pressure inside the bubbles is given for example by Ronchi's equation of state [62], or even by the hard sphere equation of state. Some experimental results suggest, however, that theoretical equations of state give too high values for ultimately dense noble gases [63]. The difficulties in finding the correct equation of state for solid state xenon in reactor temperatures hinders any reliable evaluation of the effect of possible thermal resolution or bubble growth by the dislocation loop punching mechanism on the overall intragranular bubble behaviour.

The large over-pressure in the bubbles has most probably induced the dislocation loop punching in transient tested fuel, seen as high dislocation density surrounding the large, 300 nm size bubbles [40]. However, there is no experimental data available for quantifying the changes in the bubble radius due to loop punching. Trinkhaus [63] has published a simple correlation for the required gas pressure, p_{LP}, in the bubbles for dislocation loop punching:

$$p_{LP} = \frac{2\gamma + \mu b}{r} \quad 2b \leqslant r \leqslant 10b,$$
$$p_{LP} = \frac{2\gamma}{r} + 0.2\mu \quad r > 10b, \tag{20}$$

where γ is the surface energy of UO_2, r the bubble radius, b the Burgers vector and μ the shear modulus. For transient tested fuel in Ref. [40] it can be well assumed that the pressure in the large bubbles was limited by the dislocation loop punching process. Eq. (20) would then give a pressure of about 14 GPa for larger bubbles. This is about the same pressure which would be given by Ronchi's equation of state for xenon of 5.5 g/cm^3 density at 1400 K. The measured gas densities in the bubbles are close to this, but remembering the uncertainty in the equation of state it is concluded that the information is not adequate for modelling dislocation loop punching.

2.6. Coefficient b in Eq. (7)

Baker has reported results of measurements for the bubble size dependence on the fuel temperature in steady state irradiation at 7.9 MWd/kgU [39]. Narrow size distribution is an outstanding feature in the data; at these burn-ups no large bubbles are reported. The bubble size as a function of burn-up is calculated with Eq. (18), using the bubble density in Eqs. (10), (12) and (13). The fission rate is constant, 10^{13} cm^{-3}/s and 0.26 stable gas atoms are assumed to be generated per fission. The gas density in the bubbles is 4 g/cm^3. The measured and calculated bubble sizes are presented in Fig. 6. The value 3×10^{-17} cm^3 for coefficient b in Eq. (7) seems to reproduce the bubble data fairly well.

At low temperatures the population of small bubbles exists up to very high burn-up. Using the value of

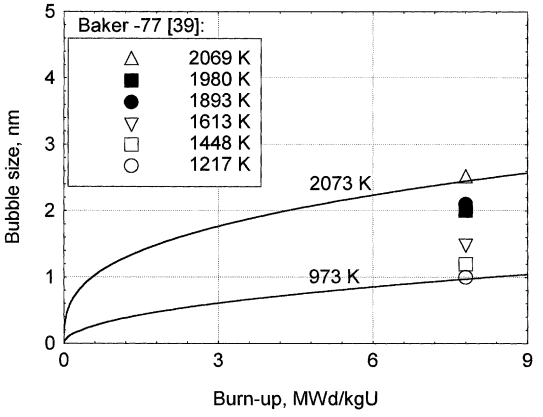

Fig. 6. Calculated and measured [39], bubble size in low burn-up irradiation.

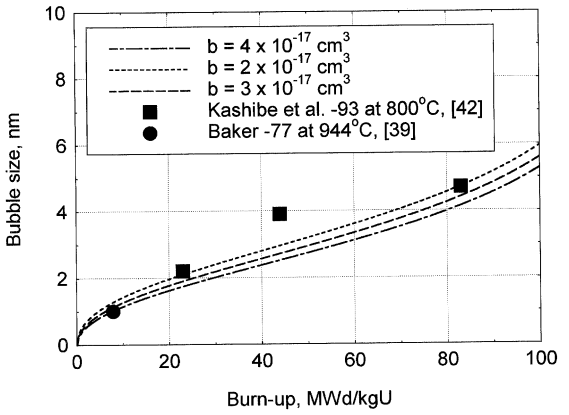

Fig. 7. Calculated and measured [39,42], bubble size in low temperature and high burn-up irradiation.

3×10^{17} cm^3 for coefficient b in Eq. (7) is found to predict reasonably well the data on bubble radius by Baker and Kashibe et al. in 800 °C. This is illustrated in Fig. 7, where the calculated bubble size by Eq. (18) is presented together with experimental data points.

2.7. Grain boundary layer

After the gas atoms have diffused to the grain boundaries, they may be resoluted back to the grain by collisions with energetic fission fragments in a manner similar to the resolution from intragranular bubbles. The resolution of gas from the grain boundaries has an effect on the evolution of the gas concentration profile in the grain. In a narrow layer at the grain periphery the resolution of the grain boundary gas is modelled by increasing the gas generation rate with a term β_{add}:

$$\beta = \beta + \beta_{\text{add}} = \beta + \frac{4\pi r_0^2 N b' F}{2V} \approx \beta + \frac{N b' F}{4\lambda}, \tag{21}$$

where N is the gas content per unit area at the grain boundary, b' the probability of gas atoms to be resoluted from grain boundary bubbles by a fission event, F the fission density, λ the average penetration depth of the resoluting gas atoms and V the volume of the resolution layer. The resoluting gas atoms are assumed equally distributed in volume V, which is a good approximation for a thin resolution layer [66]. The kinetics of the evolution of the grain boundary gas are accounted for by the equation

$$\frac{\partial N(t)}{\partial t} = -2D \frac{\partial c(r_{\text{g}}, t)}{\partial r_{\text{g}}}\bigg|_{r_{\text{g}}=r_0} - b' F N(t), \tag{22}$$

when the concentration at the grain boundary is below the saturation concentration.

Modelling the behaviour of the grain boundary gas is not the subject of this paper, but it is necessary to define the saturation concentration for testing the solution method. One way of calculating the saturation concentration, N_{sat}, at the grain boundaries is to assume lenticular grain boundary bubbles containing ideal gas. The pressure in the bubbles is in an equilibrium with the sum of the surface tension associated with the bubble surface specific energy, γ, and with the externally applied hydrostatic pressure, p_{ext}. The saturation concentration is then obtained by [64]

$$N_{\text{sat}} = \frac{4 f_{\text{c}} f(\theta) r_{\text{b}}}{kT \sin^2\theta}\left(\frac{2\gamma}{r_{\text{b}}} + p_{ext}\right), \qquad f(\theta) = 1 - 1.5\cos(\theta) + 0.5(\cos(\theta))^3, \tag{23}$$

where f_{c} is the fractional coverage of the grain boundary area by the lenticular bubbles, $f(\theta)$ is the ratio of the volumes of lenticular and spherical bubbles of radius r_{b}, k is Boltzmann's constant, T the temperature in Kelvin, the surface energy and θ is the dihedral angle. The following values are applied in the calculations:

$$f_{\text{c}} = 0.7, \quad \theta = 50°, \quad r_{\text{b}} = 0.5\ \mu\text{m}, \quad \gamma = 1\ \text{J/m}^2, \quad p_{\text{ext}} = 10\ \text{MPa}.$$

3. Solution method

The set of equations to be solved under time varying conditions is composed of the basic diffusion Eq. (1) with a collection of accompanying equations presented in the previous chapter to account for the irradiation effects and the bubble precipitation induced by the low solubility of the fission gases in UO_2 matrix. The strategy is to assume the irradiation conditions constant during the time step. Rapidly changing conditions can be tackled by dividing the irradiation history into sufficiently short periods. This does not lead to excessive computing times, since the applied algorithm requires inherently short time steps; long steps given as input are cut into suitable lengths to ensure convergence and accuracy of results.

3.1. The locally accurate method (LOAM)

The method presented earlier [65,66], is extended to account for the gas precipitation into and resolution from intragranular bubbles. In the basic method the spherical grain is divided into nodes of equal volume. The boundaries of the nodes are then defined by their number, N_x:

$$\frac{r_{i,i+1}}{r_0} = \left(\frac{i}{N_x}\right)^{1/3}, \tag{24}$$

where r_0 is the radius of the grain and $r_{i,i+1}$ is the radius at the boundary between nodes number i and $i+1$.

The concentration is calculated in the centres of the nodes as a sum of the contributions of narrow slices around the node points:

$$c(r_i,t^{m+1})=\sum_{n=1}^{N}\left(c_0\left[r_a+\frac{r_b-r_a}{N}\left(n-\frac{1}{2}\right),t^m\right]A_n\right), \tag{25}$$

where $c_0(r,t^m)$ is the average concentration in the narrow slice at the beginning of time step m, r_a and r_b are the smaller and larger radii of the surrounding volume affecting the concentration at r_i, N is the number of the narrow slices and A_ns are constants. The contribution of the slices in an infinite sphere is very well approximated by the Gaussian distribution, if the radius r_i is clearly larger than zero and the standard deviation is small compared to r_i. In spherical co-ordinates the maximum of the Gaussian distribution is shifted from r_i to r_x:

$$r_x=\frac{r_i+\sqrt{r_i^2+8D\Delta t}}{2}, \tag{26}$$

which means that $(r_a+r_b)/2$ is r_x and not r_i, as might be first estimated. The radii r_a and r_b are selected so that the contribution of $c_0(r_a,t^m)$ and $c_0(r_b,t^m)$ to $c(r_N,t^{m+1})$ is extremely low, in the order of c_0 times the value of normal distribution at $\pm3\sigma$.

The maximum length of the time step by using only three radial nodes can be calculated as

$$\Delta t=\frac{8.1\times10^{-5}r_0^2}{D}. \tag{27}$$

The distribution between the node points is approximated by quadratic functions. The values and the first derivatives of the functions are equal at the boundaries of adjacent nodes. The gas generated during the time step is in the base method simply added to the calculated concentration, since the effect of the diffusion of that gas is negligible under these conditions [65].

3.2. LOAM with bubble precipitation

The presence of bubble precipitation complicates the solution. The precipitation rate given by Eq. (7) has to be subtracted from Eq. (1). The radius $\bar{r}$ in Eq. (7) is approximated with the radius of a bubble with average volume in the beginning of the time step. The concentration in the matrix, $c(r_i,t)$, used in Eq. (7) is obtained from

$$c(r_i,t)=\hat{c}(r_i,t^{m+1})+\beta t-\Delta m(r_i,t), \tag{28}$$

where $\hat{c}(r_i,t^{m+1})$ is the concentration calculated by Eq. (25). Thus, the diffusion of the gas in the matrix at the beginning of the time step is already accounted for in the calculation of the change in the concentration induced by precipitation. The bubble density is calculated as an average during the time step:

$$\overline{C}_b=\frac{\int_0^{\Delta t}C_b(t)\,dt}{\Delta t}. \tag{29}$$

C_b is calculated with Eqs. (8)–(13) for low temperature – low burn-up fuel and with Eqs. (16) and (17) for high temperature – high burn-up fuel. Eq. (15) is used to determine which set of equations is applied. Eq. (7) becomes then

$$\frac{dm(r_i,t)}{dt}=4\pi\bar{r}(r_i,t)D\left[c(r_i,t^{m+1})+\beta t-(m(r_i,t)-m(r_i,t_0))\right]\overline{C}_b(r_i,t)-Fbm(r_i,t). \tag{30}$$

The solution for this is

$$m(r_i,t)=m(r_i,t_0)e^{-Bt}+\frac{C}{B^2}\left(e^{-Bt}-1\right)+\frac{C}{B}t-\frac{A}{B}\left(e^{-Bt}-1\right), \tag{31}$$

where

$$\begin{aligned}A&=4\pi\bar{r}D\overline{C}_b(c(r_i,t_0)+m_0(r_i,t_0)),\\ B&=4\pi\bar{r}D\overline{C}_b+Fb,\\ C&=4\pi\bar{r}D\overline{C}_b\beta.\end{aligned} \tag{32}$$

The boundary conditions are

$$\begin{aligned}&\frac{\partial c(r_g,t)}{\partial r}=\frac{\partial m(r_g,t)}{\partial r}=0\quad\text{at } r=0,\\ &c(r_g,t)=m(r_g,t)=0\quad\text{at } r=r_0.\end{aligned} \tag{33}$$

The gas concentration in the bubbles, m, as a function of grain radius is approximated by quadratic functions between the nodal points.

The amount of released gas from the grains as a function of time, $Q(t)$, is calculated as

$$Q(t)=1-\frac{G_{in}}{G_{gen}}=1-\frac{\int_0^{r_0}c(r_g,t)\,dr+\int_0^{r_0}m(r_g,t)\,dr}{\int_0^t\beta(t)\,dt}. \tag{34}$$

The accuracy of the LOAM with and without grain boundary resolution has been checked against analytical solutions in the previous papers [65,66]. The accuracy of the LOAM with bubble precipitation and resolution is checked against fourth order Runge–Kutta method with an adaptive step size algorithm [67], where the grain is divided into 65 radial nodes. The four point Runge–Kutta with adaptive step size control with the same spatial discretisation as applied in this paper has proven to be very accurate [21]. The parameters applied are given in Table 2. The bubble density is constant in this example calculation. The results are illustrated in Fig. 8.

Table 2
Parameters for checking the solution against the Runge–Kutta method

b	3×10^{-17} l/s
Grain radius	5 μm
$C_b(r,t)$	5×10^{17} bubbles/cm^3
β	0.26×10^{13} atoms/cm^3 s
D	3.028×10^{-19} m^2/s

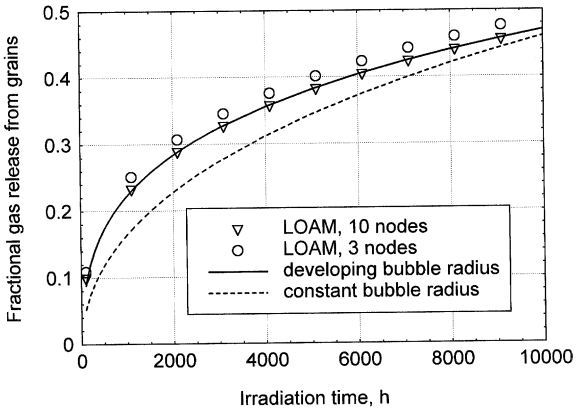

Fig. 8. Fission gas release fractions from grains in steady state irradiation calculated by the present method (LOAM) and the Runge–Kutta method assuming developing bubble size. An additional release curve is calculated by Runge–Kutta method assuming constant bubble size.

The solution with only three nodes overestimates the release slightly, but an excellent correspondence is achieved by using 10 nodes.

The results of a calculation where the intragranular bubble radius is assumed to be constant during the irradiation, 1 nm, is included in Fig. 8. There is quite a noticeable difference between the release by this approach and the more accurate method. The error would become even larger, if the changes in the bubble concentration as a function of burn-up and temperature were applied.

3.3. LOAM with bubble precipitation and grain boundary resolution

If resolution from the grain boundaries is accounted for, the concentration at the boundary of the resolution layer, at $r = r_\lambda$, is calculated in addition to the concentrations at the centres of the isovolume nodes. The division of the grain into nodes is slightly changed: r_0 in Eq. (24) is replaced by r_λ:

$$r_\lambda = r_0 - 2\lambda, \tag{35}$$

where λ is the average penetration depth of gas atoms resoluting from the grain boundary. The concentration within the resolution layer is approximated by a quadratic polynomial. The resolution layer is thin compared with the grain radius, and therefore a one-dimensional diffusion equation can be used within the layer:

$$\frac{\partial c(r_g,t)}{\partial t} = D\frac{\partial^2 c(r_g,t)}{\partial r_g^2} + \beta(t) - \frac{\partial m(r_g,t)}{\partial t}. \tag{36}$$

Eq. (36) is integrated over the time step and spatially over the resolution layer. The definition of Eq. (21) is used for the gas generation rate. Eq. (22) is solved for obtaining the concentration of the grain boundary gas as a function of time by assuming the spatial derivative to be constant:

$$\begin{aligned} N(t) &= N_0 e^{-b'Ft} - \left.\frac{\partial c}{\partial r}\right|_{r=r_0} \frac{2D}{b'F}\left(1 - e^{-b'Ft}\right) && N(t) < N_{sat}, \\ N(t) &= N_{sat} && N(t) = N_{sat}, \end{aligned} \tag{37}$$

where N_0 is the concentration at the grain boundary in the beginning of the time step. Integration of Eq. (36) before saturation at the grain boundaries yields

$$\begin{aligned} \Delta G_{res} = D\Bigg[& 4\pi r_0^2 \int_{t_0}^{t_0+\Delta t} \left(\left.\frac{\partial c}{\partial r}\right|_{r=r_0}\right) dt \\ & - 4\pi r_\lambda^2 \int_{t_0}^{t_0+\Delta t} \left(\left.\frac{\partial c}{\partial r}\right|_{r=r_0-2\lambda}\right) dt \Bigg] + FyV\Delta t \\ & + \frac{b'FV}{4\lambda}\Bigg[\frac{N_0}{b'F}\left(1 - e^{-b'F\Delta t}\right) - \frac{2D}{b'F}\left.\frac{\partial c}{\partial r}\right|_{r=r_0}\Delta t \\ & - \frac{2D}{(b'F)^2}\left.\frac{\partial c}{\partial r}\right|_{r=r_0}\left(e^{-b'F\Delta t} - 1\right)\Bigg] \\ & - (\overline{m}(\Delta t) - \overline{m}_0)V, \end{aligned} \tag{38}$$

where ΔG_{res} is the change in the gas content in the matrix in the resolution layer, y the fission yield of stable gas atoms, V the volume of the resolution layer and $\overline{m}_0$ the average gas concentration precipitated in the bubbles in the resolution layer at the beginning of the time step. The spatial derivatives in Eq. (38) are assumed time independent in the same way as in the derivation of the solution of $N(t)$ in Eq. (37). The spatial derivatives are taken at the end of the time step; the method is therefore implicit by nature.

Since the bubbles are assumed to be immobile, the gas concentration in the bubbles can be modelled independent on radius in the thin resolution layer. Eq. (7) is used for calculating the change in the average concentration in the bubbles, $\overline{m}(\Delta t)$, in the resolution layer:

$$\frac{\partial \overline{m}}{\partial t} = 4\pi \bar{r} D \bar{c} \overline{C}_b - Fb\overline{m}, \tag{39}$$

where the concentration in the matrix, $\bar{c}$, is the time dependent spatial average in the resolution layer:

$$\begin{aligned}\overline{c} &= \overline{c}(t)\\ &= \overline{c}_0 + \int_0^t \left(\beta + \frac{b'FN(t)}{4\lambda} + \left.\frac{\partial c}{\partial r}\right|_{r=r_0} \frac{4\pi D r_0^2}{V} \right.\\ &\quad \left. - \left.\frac{\partial c}{\partial r}\right|_{r=r_\lambda} \frac{4\pi D r_\lambda^2}{V}\right) \mathrm{d}t - \int_0^t \mathrm{d}\overline{m}. \end{aligned} \tag{40}$$

Integration of Eq. (40) yields

$$\begin{aligned}\overline{c}(t) = \overline{c}_0 &+ \left[\beta + \left.\frac{\partial c}{\partial r}\right|_{r=r_0} \frac{4\pi D r_0^2}{V} - \left.\frac{\partial c}{\partial r}\right|_{r=r_\lambda} \frac{4\pi D r_\lambda^2}{V} \right.\\ &\left. - \left.\frac{\partial c}{\partial r}\right|_{r=r_0} \frac{D}{2\lambda}\right] t + \frac{b'F}{4\lambda}\left[\frac{N_0}{b'F}\left(1 - \mathrm{e}^{-b'Ft}\right)\right.\\ &\left. + \left.\frac{\partial c}{\partial r}\right|_{r=r_0} \frac{2D}{(b'F)^2}\left(1 - \mathrm{e}^{-b'Ft}\right)\right] - (\overline{m}(t) - \overline{m}_0), \end{aligned} \tag{41}$$

where $\overline{c}_0$ is the average concentration in the matrix in the resolution layer in the beginning of the time step.

Eq. (41) is inserted in Eq. (39), which is solved for $\overline{m}(\Delta t)$:

$$\begin{aligned}\overline{m}(\Delta t) = m_0 \mathrm{e}^{-(A+B)\Delta t} &+ \frac{AJ}{A+B}\Delta t + \frac{AJ}{(A+B)^2}\left(\mathrm{e}^{-(A+B)\Delta t} - 1\right)\\ &+ \frac{A\overline{c}_0}{A+B}\left(1 - \mathrm{e}^{-(A+B)\Delta t}\right)\\ &+ \frac{AN_0}{4\lambda(A+B-b'F)}\left(\mathrm{e}^{-(A+B+b'F)\Delta t} - \mathrm{e}^{-b'F\Delta t}\right)\\ &+ \frac{DAc'_{r_0}}{2\lambda b'F(A+B)}\left(1 - \mathrm{e}^{-(A+B)\Delta t}\right)\\ &+ \frac{DAc'_{r_0}}{2\lambda b'F(A+B-b'F)}\left(\mathrm{e}^{-(A+B-b'F)\Delta t} - \mathrm{e}^{-b'F\Delta t}\right)\\ &+ \frac{m_0 A}{A+B}\left(1 - \mathrm{e}^{-(A+B)\Delta t}\right), \end{aligned} \tag{42}$$

where

$$\begin{aligned} A &= 4\pi \bar{r} D \overline{C}_\mathrm{b},\\ B &= Fb,\\ J &= \beta + c'_{r_0}\frac{4\pi D r_0^2}{V} - c'_{r_\lambda}\frac{4\pi D r_\lambda^2}{V} - c'_{r_0}\frac{D}{2\lambda},\\ c'_{r_0} &= \left.\frac{\partial c}{\partial r}\right|_{r=r_0},\\ c'_{r_\lambda} &= \left.\frac{\partial c}{\partial r}\right|_{r=r_\lambda}. \end{aligned}$$

The spatial derivatives in Eq. (42) are assumed to be constant during the time step. They are expressed in terms of the coefficients of the quadratic functions approximating the concentration profile in the resolution layer at the end of the time step $n \to n+1$:

$$\begin{aligned} \left.\frac{\partial c}{\partial r}\right|_{r_\lambda}^{n+1} &= 2c_0^{n+1} r_\lambda + b_0^{n+1},\\ \left.\frac{\partial c}{\partial r}\right|_{r_0}^{n+1} &= 2c_0^{n+1} r_0 + b_0^{n+1}. \end{aligned} \tag{43}$$

Eq. (42) is implemented to Eq. (38), where ΔG_res is set equal to the change in the gas content in the matrix in the resolution layer expressed in terms of the quadratic function f_λ approximating the concentration profile at time t^n and t^{n+1}:

$$\Delta G_\mathrm{res} = \int_{r_0-2\lambda}^{r_0} 4\pi r^2 (f_\lambda^{n+1} - f_\lambda^n)\,\mathrm{d}r. \tag{44}$$

The following conditions prevail at the boundaries of the resolution layer:

$$\begin{aligned} \left.\frac{\mathrm{d}f_\lambda}{\mathrm{d}r}\right|_{r=r_\lambda} &= \left.\frac{\mathrm{d}f_N}{\mathrm{d}r}\right|_{r=r_\lambda},\\ f_\lambda(r_\lambda) &= f_N(r_\lambda),\\ f_\lambda(r_0) &= 0, \end{aligned} \tag{45}$$

where f_N is the quadratic polynomial describing the concentration between r_N and r_λ, where N is the number of equal volume nodes. Eqs. (44) and (45) together with the boundary conditions (33) form a set of linear equations, where the unknowns are the coefficients for the polynomials f_N and f_λ. The equations are solved analytically and the concentration at r_λ is then directly calculated from the coefficients. The average concentration in the bubbles in the resolution layer is obtained by using Eq. (42). The concentration in the bubbles at r_λ is calculated by assuming the concentration in the bubbles to be a quadratic function in the resolution layer and that the quadratic functions obey the conditions defined by Eq. (45).

If the saturation concentration in the grain boundaries has been reached, the $N(t)$ is replaced by N_sat in Eqs. (40) and (36), which simplifies the solution somewhat.

The amount of released gas from the grains as a function of time is finally calculated by Eq. (34). The variables to be stored from one time step to another are the concentrations in the matrix and in the bubbles at the middle of the nodal points and at r_λ.

3.3.1. Results

The model and the solution method were tested with 700 cases. The first 699 cases were for checking the convergence and accuracy of the solution. The last case included tens of thousands of time steps for obtaining information on the required computing time. The power histories had time steps with constant fission rates and constant diffusion coefficients. The temperature for each time step was chosen randomly between 900 °C and the maximum temperature T_max allowed for the particular

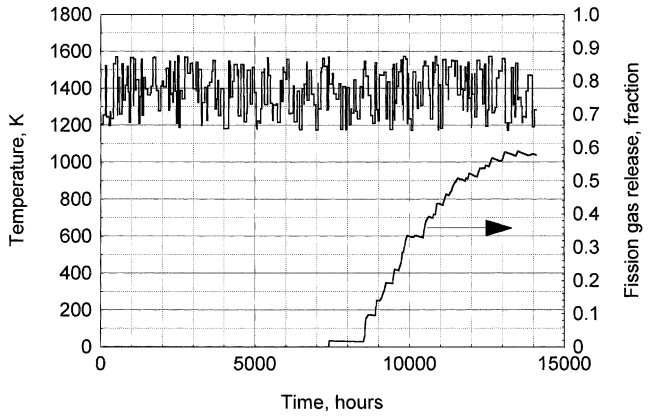

Fig. 9. An example of a temperature history and the calculated fission gas release by LOAM with grain boundary resolution and intragranular gas precipitation.

history. The maximum temperature was predetermined randomly between 900 and 1900 °C to produce a wide distribution of release fractions. The fission rate, F, was calculated from the temperature for each time step:

$$F = \left[0.857 + \frac{T - 900}{700}\right] \times 10^{13} \ \frac{\text{fissions}}{\text{cm}^3\,\text{s}}, \tag{46}$$

where the temperature T is in degrees centigrade.

The length of each time step varied between 0.1 and 100 h. On the average 221 time steps were included in a power history. The total number of time steps exceeded 147 000. An example of a temperature history and the calculated fission gas release are shown in Fig. 9.

The grain was divided into either three or 10 nodes. Increasing the number of nodes above 10 had only an insignificant effect on the results, and the calculations with 10 radial nodes were considered accurate. When only three nodes were used, the solution had a tendency to diverge or oscillate in the resolution layer. This problem was remedied by slowing down the changes in concentrations at r_λ:

$$\begin{aligned} c_{r\lambda}^{n+1} &= \frac{c_{r\lambda}^{n+1} + c_{r\lambda}^{n}}{2}, \\ m_{r\lambda}^{n+1} &= \frac{m_{r\lambda}^{n+1} + m_{r\lambda}^{n}}{2}. \end{aligned} \tag{47}$$

The calculated release fractions with 10 nodes as a function of the release fractions with three nodes are shown in Fig. 10. A slight over-prediction by using three nodes is more visible in Fig. 11, where the difference between the calculated release fractions is plotted as a function of the release fractions by three nodes. This over-prediction is due to the fact that three nodes were not adequate to represent perfectly the concentration profile in the grain [13,66]. A correction was introduced to achieve a better agreement:

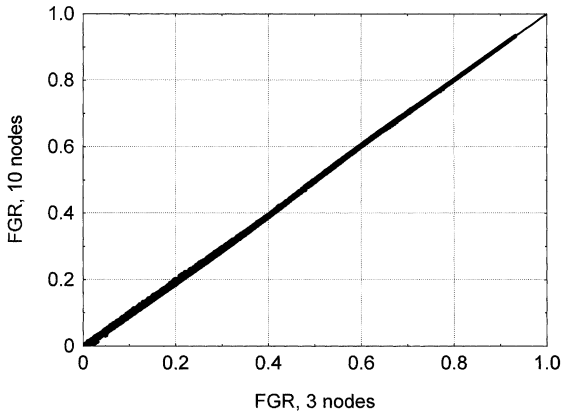

Fig. 10. Calculated release fractions in 699 test cases by LOAM using 10 nodes as a function of the release fractions with three nodes.

$$\begin{aligned} &\text{FGR}_{3c} = 0.7\text{FGR}_3, && \text{FGR}_3 \leqslant 0.02, \\ &\text{FGR}_{3c} = 0.983\text{FGR}_3 - 0.00566, && 0.02 < \text{FGR}_3 < 0.38, \\ &\text{FGR}_{3c} = 1.061\text{FGR}_3 - 0.03518, && 0.38 \leqslant \text{FGR}_3 < 0.6, \\ &\text{FGR}_{3c} = 0.9929\text{FGR}_3 + 0.00568, && 0.6 < \text{FGR}_3 < 0.8, \\ &\text{FGR}_{3c} = \text{FGR}_3, && \text{FGR}_3 \geqslant 0.8, \end{aligned} \tag{48}$$

where FGR_{3c} is the corrected release fraction and FGR_3 is the release fraction calculated with three nodes. A test quantity named ΔFGR was chosen for evaluating the performance of LOAM with three nodes:

$$\Delta\text{FGR} = \text{FGR}_{3c} - \text{FGR}_{10}, \tag{49}$$

where FGR_{10} is the gas release fraction calculated with ten nodes. In Fig. 12 the test quantity ΔFGR is plotted versus FGR_3. More than 99% of the points are within $\pm 1\%$ band around the expected zero value.

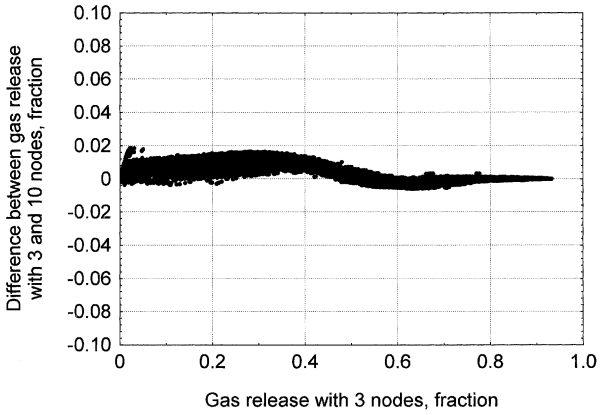

Fig. 11. The difference between release fractions calculated by LOAM using three and 10 nodes as a function of the release fractions using three nodes.

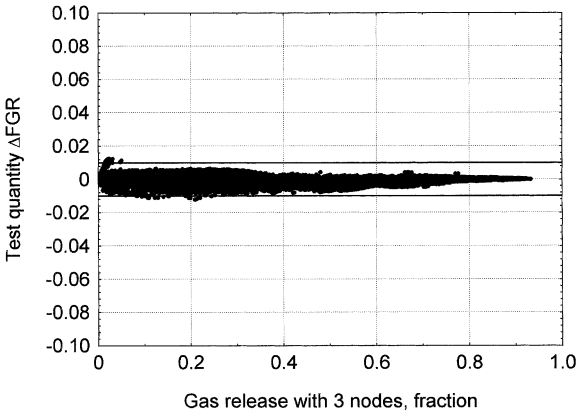

Fig. 12. The test quantity ΔFGR as a function of the release fractions by three nodes.

The computing time required by the LOAM with grain boundary resolution and bubble precipitation was tested against the LOAM without bubble precipitation. A temperature history consisting of more than 9000 time steps was used in the comparison. The inclusion of the bubble precipitation almost doubled the calculation time, if the same diffusion coefficient was used by the two versions. Taking into account the fact that the LOAM with bubble precipitation requires atomic diffusion coefficient instead of an effective one, the real difference between the computing times would be slightly above 100%. This is not crucial for the use of the model with bubble precipitation, since

1. The computing times are still clearly of the same order of magnitude.
2. As the rule the performance of computer processors doubles every 18 months.
3. The calculation of the fission gas release consumes only a small part of the total computing time required for a complicated integral fuel performance code.

4. Discussion

Detailed models for fission gas release have their pros and cons. Complex models demand more computing power and storage capacity compared with simple models, which favours the latter. Another argument that has been used against detailed models is the amount and nature of parameters required. If too many parameters are involved, many of them can be considered fitting constants rather than physical quantities.

The advantage of detailed models is the possibility to include more phenomena, thus enabling a better correspondence to physical reality. For example the effect of decreasing bubble density with increasing burn-up, especially in high temperatures, on the fission gas release is difficult to model by using only a temperature dependent effective diffusion coefficient. The effective diffusion coefficient tends to increase with burn-up accumulation, since the decreasing bubble concentration at high burn-ups results in increasing fraction of the gas remaining in the fuel matrix. The attenuation of the effective diffusion coefficient in high burn-up and high temperature fuel due to the precipitation of intragranular bubbles is damped by drastic coarsening of the bubble population.

The requirement for reasonable computing times is a prerequisite for including a model in an integral fuel performance code. Detailed models are often used as stand-alone versions for parameter testing. Nevertheless, the continuously improving performance of personal computers will favour detailed mechanistic models also in integral fuel codes. However, a lot of data is definitely needed for tuning the parameters in models that have as

many details as the one presented in this paper. The model is clearly of a mechanistic nature, although it includes a few simple qualitative correlations for characterising the intragranular bubble population. The presented solution method for the set of equations supports the inclusion of many kinds of functions for the bubble density and size distribution.

A calculation of the fission gas release as a function of the pellet radius for a fictitious LWR pellet was carried out as an example of the usefulness of the present model. The linear power of the pellet is constant in time. The pellet centreline and peripheral temperatures as a function of irradiation time are shown in Fig. 13. The temperature as a function of pellet radius is assumed to be parabolic. In a real LWR pellet the temperature profile deviates from the parabolic approximation at high exposures, which would somewhat change the absolute release values. The retained fission gas in the pellets at the end of irradiation is shown in Fig. 14. The steps in the radial profile are a consequence of release at different times. This kind of steps in the radial retention curves have been observed in many experiments [4, 48,49]. If the same example were calculated by using

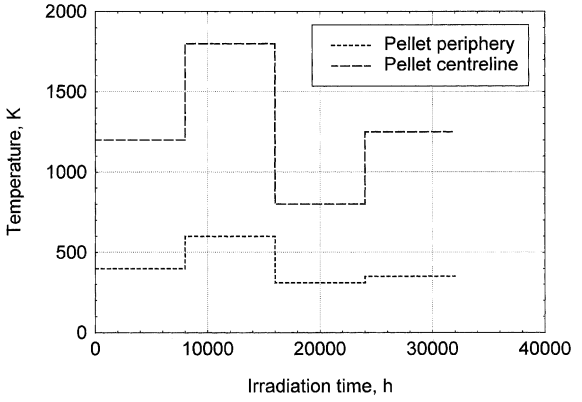

Fig. 13. The pellet centreline and peripheral temperatures of a fictitious LWR pellet as a function of irradiation time for a test calculation.

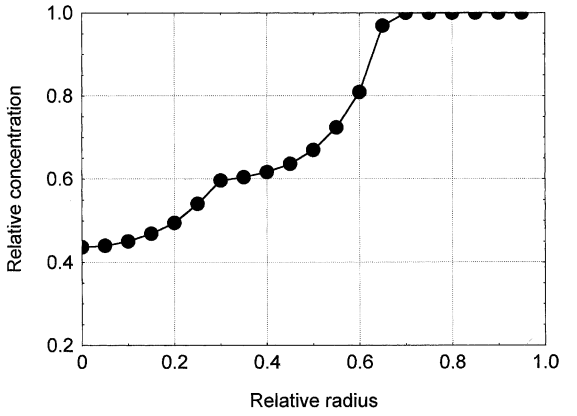

Fig. 14. Calculated retention of fission gas as a function of pellet radius at the end of irradiation for the fictitious LWR fuel.

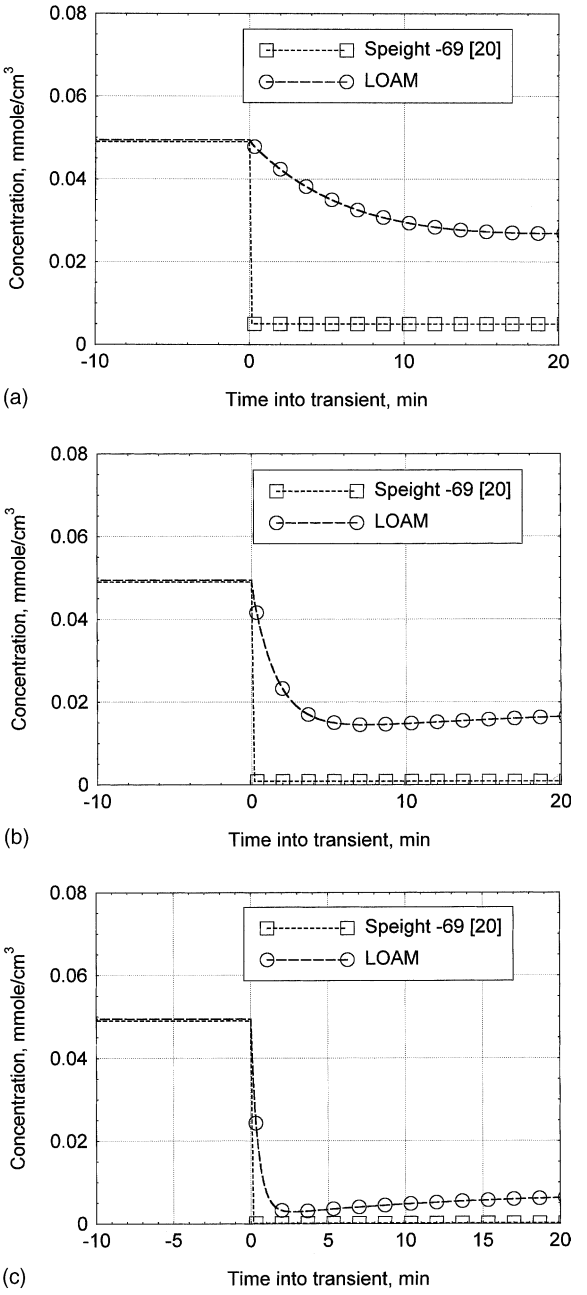

Fig. 15. Gas concentration at the inner boundary of the resolution layer in sudden temperature increase to (a) 1300 °C, (b) 1500 °C and (c) 1700 °C after 15,000 h irradiation at low temperature.

Table 3
Parameters for the sensitivity analysis

Parameter	Base value	Lower value	Upper value
Diffusion coefficient, cm^2/s	Eq. (3)	0.5 × Base value	2 × Base value
Coefficient b in Eq. (6), cm^3	3×10^{-17}	2×10^{-17}	4×10^{-17}
Threshold temperature for bubble coarsening	Eq. (15)	Base value − 100 °C	Base value + 100 °C
Gas density in bubbles, g/cm^3	4	3	5
r_F in Eq. (16), nm	100	20	200
Average penetration depth of resoluting gas atoms, nm	10	5	20
Grain size, μm	5	4.5	5.5

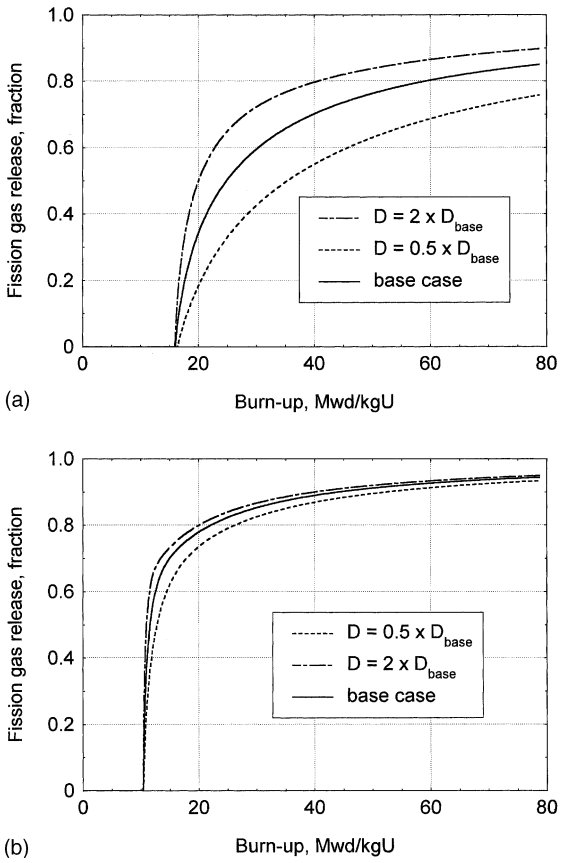

Fig. 16. The effect of varying diffusion coefficient on the calculated release fraction in steady state irradiation at (a) 1100 °C and (b) 1400 °C.

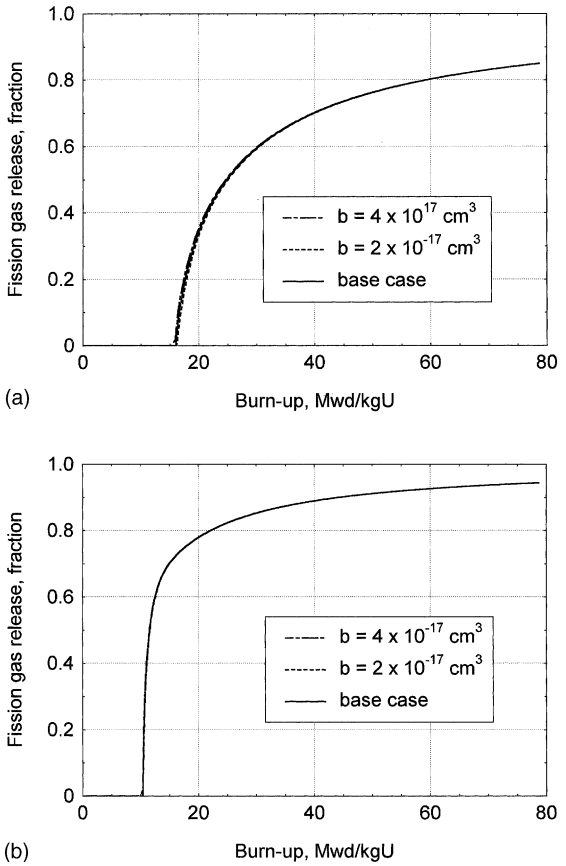

Fig. 17. The effect of changing the resolution probability from intragranular bubbles on the calculated release fraction in steady state irradiation at (a) 1100 °C and (b) 1400 °C.

only a single effective diffusion coefficient, no step in the radial gas retention curve would be produced.

The principle for dealing with the resolution layer adjacent to the grain boundary as defined in Eq. (21) is the same as for the smeared model in Ref. [64]. The gas concentration is calculated at the inner boundary of this resolution layer as $C_{\lambda\lambda}$, at

$$r = r_0 - 2\lambda, \tag{50}$$

where λ is the average penetrating depth of resoluting fission gas atoms. Another model given in [64] is called the 'Olander' model in which the resoluting fission gas atoms are supposed to be deposited a characteristic depth λ from the grain boundary. The 'Olander' model

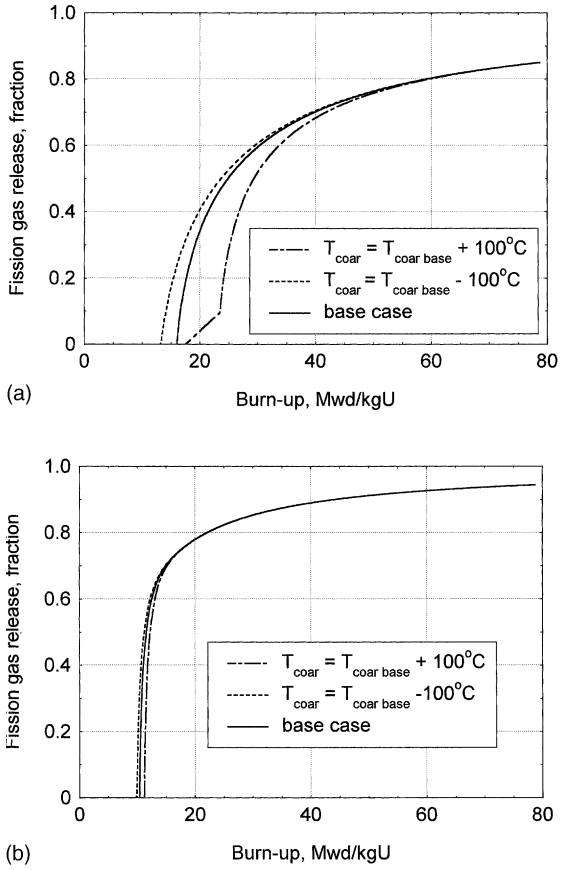

Fig. 18. The effect of modifying the threshold temperature for bubble coarsening on the calculated release fraction in steady state irradiation at (a) 1100 °C and (b) 1400 °C.

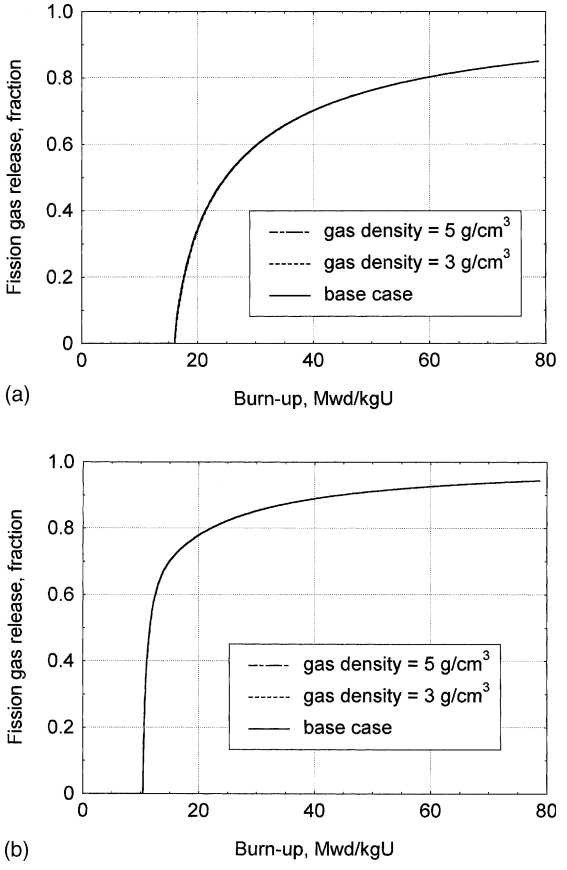

Fig. 19. The effect of varying gas density in over-pressurised intragranular bubbles on the calculated release fraction in steady state irradiation at (a) 1100 °C and (b) 1400 °C.

resembles Speight's approach [20], where the concentration at $r = r_0 - \lambda$ is calculated as

$$C_\lambda = \frac{\lambda b' F}{2D} N. \tag{51}$$

Speight's approach does not take into account the kinetics of the gas concentration at the grain boundary layer: the concentration C_λ is always inversely proportional to the diffusion coefficient. In LOAM the kinetics of the evolution of the gas concentration in the boundary layer is calculated with Eqs. (21), (22) and (38). The differences between Speight's approach and the LOAM in transients were studied in cases where the temperature was suddenly increased to 1300, 1500 and 1700 °C after 15,000 h irradiation at low temperature. The concentrations C_λ and $C_{\lambda\lambda}$ as a function of time into transient in the first 20 min are shown in Fig. 15(a)–(c). Speight's equation naturally gives an immediate decrease in C_λ, whilst the $C_{\lambda\lambda}$ calculated by the LOAM decreases smoothly. The decrease in $C_{\lambda\lambda}$ occurs faster when the temperature is increased. After the initial decrease the $C_{\lambda\lambda}$ starts increasing again in 2–20 min. This increase is associated with a large amount of gas entering the matrix from intragranular bubbles as the coarsening process begins. The $C_{\lambda\lambda}$ finally approaches C_λ in a few hours in the transient. This example clearly shows the importance of accounting for the kinetics in calculations of gas concentration in the grain boundary layer in transients.

Inaccuracies in simulating a physical phenomenon can be related to an imperfect physical model, poor knowledge of values for parameters or to the mathematical solution method. The last of these three reasons was excluded from this exercise, as shown in the previous chapter. The sensitivity analysis below reveals the relative effect of some parameters affecting the behaviour of intragranular gas on the fission gas release. The analysis discovers also possible areas of improvement in the physical model, i.e. whether empirical modelling of some phenomena would be crucial for the overall validity of the model.

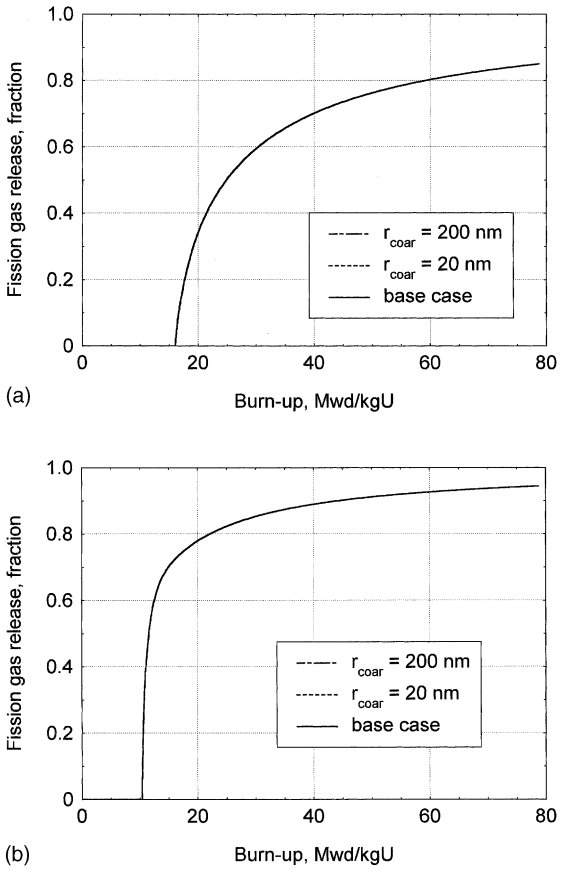

Fig. 20. The effect of the average radius of the coarsened bubbles on the calculated release fraction in steady state irradiation at (a) 1100 °C and (b) 1400 °C.

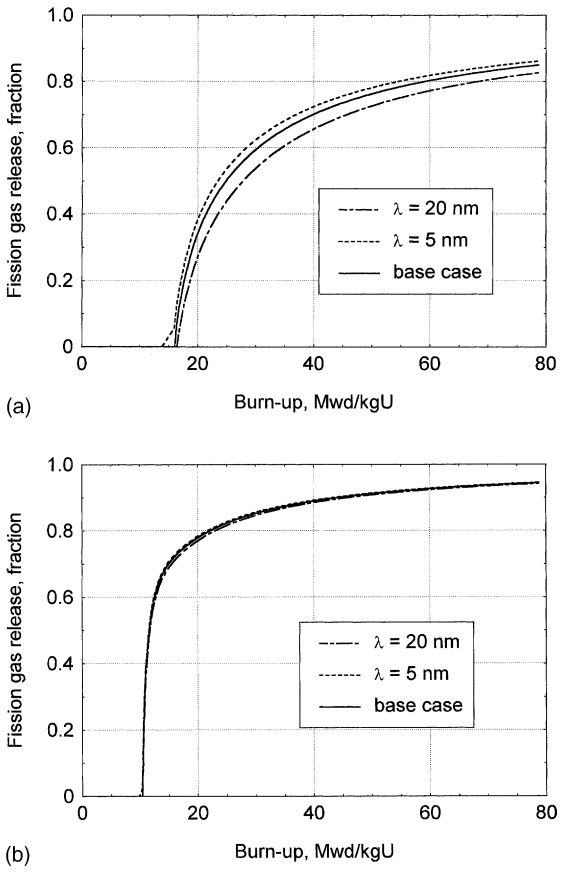

Fig. 21. The effect of doubling or halving the average penetration depth of resoluting gas atoms at the grain boundary on the calculated release fraction in steady state irradiation at (a) 1100 °C and (b) 1400 °C.

4.1. Sensitivity analysis

The effect of varying the values of different parameters in the model are of special interest in the evaluation of the performance of the model. The key parameters affecting the calculated gas release values can be singled out and the selection of a suitable compromise between the accuracy of the solution method and the computing time is made possible. The parameters to be varied to find out their relative effect on the results are listed in Table 3 together with the base, upper and lower values. The parameters are naturally not completely independent, for example the resolution probability from intragranular bubbles and the diffusion coefficient cannot be chosen freely to produce a bubble size equal to the observed size.

The calculations were performed for steady state conditions in 1100, and 1400 °C. The fission rate was 1×10^{13} cm^{-3}/s and 0.26 stable gas atoms were assumed to be generated per fission. The results are presented in Figs. 16–22.

The effect of varying the diffusion coefficient in general is fairly notable (see Fig. 16). At 1100 °C the effect is stronger than at 1400 °C. On the other hand, the effect of changing the resolution probability does not seem to have any visible influence on the release (Fig. 17). This is due to the dominating effect of the coarsening of the intragranular bubbles. The sink strength of the coarsened bubble population is so low that the gas atoms resolute from the coarsened bubbles fast enough not to slow down significantly the release to grain boundaries by diffusion.

The fission gas release depicted in Figs. 16 and 17 happens after the coarsening of the intragranular bubbles has begun. However, fission gas can be released also without coarsening. An example of this shown in Fig. 18, where the threshold temperature for the coarsening has been varied. The release starts without coarsening at 1100 °C, if the threshold temperature is increased (see the lowest release curve in Fig. 18(a)).

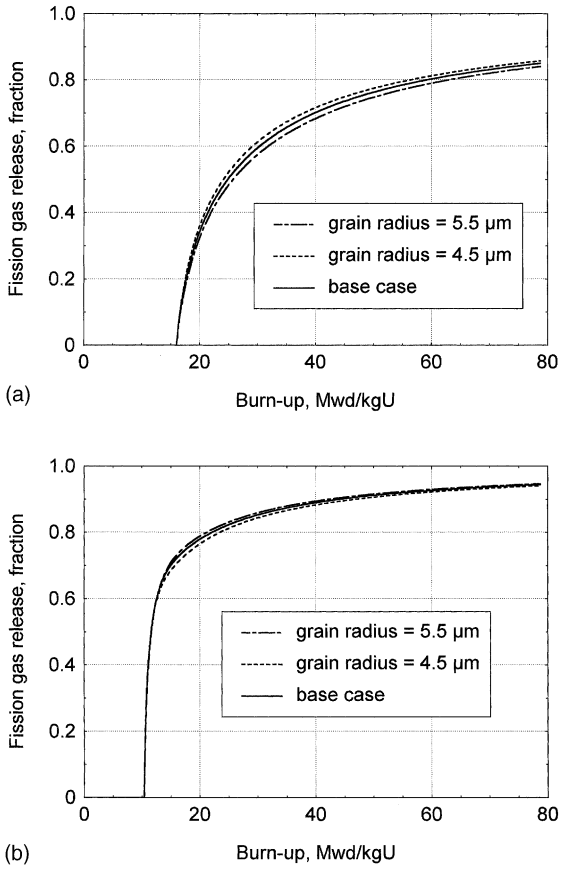

Fig. 22. The effect of varying the grain size on the calculated release fraction in steady state irradiation at (a) 1100 °C and (b) 1400 °C.

If the intragranular bubbles were assumed to be in mechanical equilibrium with the bulk solid surrounding them, the gas in larger bubbles would have a much lower density than in small bubbles [61]. The equations describing the relationship between the bubble radius and the amount of gas contained in a bubble would have to take into account the varying gas density as a function of bubble radius. However, the observed weak dependence of the gas density in intragranular bubbles on bubble radius [59,60], means that the bubble volume and thus also the amount of precipitated gas in the bubbles are approximately proportional to the third power of the bubble radius. Thus, small variations in the gas density change neither the bubble radius nor the sink strength of the intragranular bubbles very much. In this model the gas density was chosen to be constant, 4 g/cm^3, and the relationship between the bubble radius and the amount of gas in it is calculated using Eq. (18). Varying gas density in the over-pressurised bubbles between 3 and 5 g/cm^3 does not affect the release (Fig. 19).

Coarsening is obviously the most important intragranular phenomenon concerning the fission gas release. The radii of the coarsened bubbles are, according to measurements [40,43], from a few tens to a few hundreds of nanometres. The sink strength of the intragranular bubble population depends naturally on the average bubble radius. Nevertheless, the most important factor in the coarsening process is the disappearance of the small bubbles and not the exact size of the coarsened bubbles. The radii of the coarsened bubbles can vary in a wide range without any effect on the fission gas release (Fig. 20).

The impact of two physical quantities, grain size and the penetration depth of the resoluting gas atoms at the grain boundary bubbles on the release is illustrated in Figs. 21 and 22. The average penetration depth of the resoluting gas atoms at the grain boundary is difficult to measure, but doubling or halving the depth in the calculations has no large effect on the release at 1100 °C, and at 1400 °C there is no visible effect at all (Fig. 21). The grain size is an important parameter in diffusional release, since the average length of the path that the gas atoms migrate to the grain boundary depends directly on it. The grains are of varying shape and the approximation of the spherical grains introduces some inaccuracy in the calculations.

A tetracaidecahedron (TKD) is a more realistic shape of a grain in sintered UO_2 fuel than a perfect sphere [11]. The TKD has fourteen faces, six of which are square and eight hexagonal. The larger surface-to-volume (S/V) ratio of the TKD compared with a sphere of equivalent volume should result in a slightly larger release fraction from the former. The S/V ratio of a sphere is proportional to the inverse of the grain radius. The S/V ratio of the TKD is equal to the S/V ratio of a sphere whose volume is about 6% smaller than the volume of the TKD. Thus, decreasing the grain radius by 10% should result in a higher fission gas release fraction from the sphere than from the TKD of equal volume. However, changing the grain radius by 10% has only a minor effect on the release fraction, even at high release fractions, as illustrated in Fig. 22.

The diffusion coefficient and the threshold temperature for the coarsening seem to be the most important parameters in intragranular gas behaviour. Mechanistic models by migration and coalescence or Ostwald ripening provide too slow coarsening compared with experimental results. Therefore a simple empirical model was applied. Remembering the importance of the bubble coarsening on the release, an elaboration of this model might be elucidative. Nevertheless, a very sophisticated coarsening model would hardly change the results, since the sensitivity analysis revealed that the average radius of the coarsened bubbles between 20 and 200 nm plays, in practise, no role in fission gas release at the two temperatures analysed.

In general the entire model presented here does not predict large enough release for rapid transients. The

observed 90% local release in 4 h [49], could be achieved by increasing the diffusion coefficient and by modifying the grain boundary model. The importance of the grain boundary release is supported by Zacharie et al. who have estimated that most of the release from preirradiated LWR fuel comes from interlinking grain boundary bubbles during the first hour of annealing [68]. Directed bubble diffusion along the vacancy gradient could offer an alternative explanation [23,69].

The tested range for the threshold temperature for bubble coarsening was large, ±100 °C, to outline its importance. In reality the correlation for the threshold temperature can be defined more accurately. However, the validation of a whole fission gas release model would require also consideration of intergranular phenomena. The capacity of the grain boundaries to accumulate gas atoms before the interlinkage of intergranular bubbles as a function of temperature, percolation phenomena and the effect of mechanical stresses on intergranular porosity should be evaluated together with the model for intragranular gas. The behaviour of intergranular gas and the validation of the total model will be discussed in another paper.

5. Summary and conclusions

A model for fission gas release by diffusion in irradiation of sintered LWR UO_2 fuel with special emphasis on intragranular fission gas behaviour was presented, including submodels for intragranular bubble precipitation and resolution of gas atoms from the bubbles. The gas in the intragranular bubbles was modelled to be in a high pressure, which is in agreement with latest experimental results. Special treatment for significant bubble coarsening in elevated temperatures was applied. The coarsening was modelled to be triggered off at a certain burn-up dependent threshold temperature. The model was shown to predict relatively well the appearance of the bubble population compared with experiments. Example calculations showed that qualitatively a better agreement with the experiments can be obtained by using a detailed model than with a simple one.

A method introduced in an earlier paper, LOAM, for solving the set of equations was enhanced to include also the bubble behaviour. The UO_2 grain was divided into nodes of equal volume. The gas concentration in the matrix and in intragranular bubbles was calculated for each node and also for a thin layer in the surface of the grain, where the calculation of the resolution of the gas atoms from the grain boundary was integrated into the solution. The temperature and power histories were divided into time steps of constant conditions. The solution method was extensively checked for stability and accuracy. Three isovolume nodes were found to be adequate for achieving an accuracy of ±1% also for complicated power histories. The computing time of the LOAM with bubble precipitation and grain boundary resolution was acceptable for integral fuel performance codes.

The relative importance of various parameters was studied with a sensitivity analysis. The diffusion coefficient and the threshold temperature for the coarsening were the most important parameters. A final tuning of the model would require a more thorough treatment of intergranular gas, which will be the subject of another paper.

References

[1] C. Wise, J. Nucl. Mater. 136 (1985) 30.
[2] B.J. Lewis, J. Nucl. Mater. 148 (1987) 28.
[3] C. Forat, B. Blanpain, B. Kapusta, P. Guedeney, P. Permezel, Proceedings of a Technical Committee Meeting, Pembroke, Ont., Canada, 28 April–1 May 1992, IAEA-TECDOC-697, p. 68.
[4] R. Manzel, R. Eberle, International Topical Meeting on LWR Fuel Performance, ANS/ENS, 21–24 April 1991, Avignon, France, Proceedings, p. 528.
[5] J.O. Barner, M.E. Gunningham, M.D. Fresley, D.D. Lanning, International Topical Meeting on LWR Fuel Performance, ANS/ENS, 21–24 April 1991, Avignon, France, Proceedings, p. 538.
[6] F. Lemoine, M. Balourdet, Proceedings of the International Topical Meeting on LWR Fuel Performance, Portland, OR, 2–6 March 1997, ANS, p. 693.
[7] R. Manzel, M. Coquerelle, Proceedings of the International Topical Meeting on LWR Fuel Performance, Portland, OR, 2–6 March 1997, ANS, p. 693.
[8] D.R. Olander, Fundamental Aspects of Nuclear Reactor Fuel Elements. Report no. TID-26711-P1. Technical Information Centre, Office of Public Affairs, Energy Research and Development Administration, Oak Ridge, TN, 1976, p. 199.
[9] K. Lassmann, Presentation in TRANSURANUS Training Course, Institute for Transuranium Elements, Karlsruhe, Germany, 17–21 June 1996.
[10] J.A. Turnbull, Presentation in TRANSURANUS Training Course, Institute for Transuranium Elements, Karlsruhe, Germany, 17–21 June 1996.
[11] R.J. White, M.O. Tucker, J. Nucl. Mater. 118 (1983) 1.
[12] Background and Derivation of ANS-5.4 Standard Fission-Product-Release Model, NUREG/CR–2507, American Nuclear Society, 1982.
[13] J.R. Matthews, M.H. Woods, Nucl. Eng. Des. 56 (1980) 439.
[14] L. Väth, J. Nucl. Mater. 99 (1981) 324.
[15] K. Forsberg, A.R. Massih, J. Nucl. Mater. 127 (1985) 141.
[16] K. Forsberg, A.R. Massih, J. Nucl. Mater. 135 (1985) 140.
[17] P.T. Elton, K. Lassmann, Nucl. Eng. Des. 101 (1987) 259.
[18] L.C. Bernard, E. Bonnaud, J. Nucl. Mater. 244 (1997) 75.
[19] K. Lassmann, H. Benk, J. Nucl. Mater. 280 (2000) 127.
[20] M.V. Speight, Nucl. Sci. Eng. 31 (1969) 180.
[21] P. Lösönen, J. Nucl. Mater. 280 (2000) 56.
[22] J.H. Evans, J. Nucl. Mater. 210 (1994) 21.

[23] J.H. Evans, Paper presented in the International Seminar on Modelling Fission Gas Behaviour in LWR Fuel, 23–26 September 2000, Cadarache, France.
[24] J.A. Turnbull, R.J. White, C. Wise (Eds.), Proceedings of the Conf. on Water Reactor Fuel Element Computer Modelling in Steady State, Transient and Accident Conditions, Preston, UK, 18–22 Sept. 1988, p. 174, IWGFPT/32.
[25] J.A. Turnbull, C.A. Friskney, J.R. Findlay, F.A. Johnson, A.J. Water, J. Nucl. Mater. 107 (1982) 168.
[26] Hj. Matzke, Rad. Eff. 53 (1980) 219.
[27] J.R. MacEwan, W.H. Stevens, J. Nucl. Mater. 11 (1964) 77.
[28] D. Davies, G. Long, AERE Rep. No. 4347 (1963), in: J.A. Turnbull, R.J. White, C. Wise (Eds.), Proceedings of the Conf. on Water Reactor Fuel Element Computer Modelling in Steady State, Transient and Accident Conditions, Preston, UK, 18–22 Sept. 1988, pp. 174–181, IWGFPT/32.
[29] F.S. Ham, J. Phys. Chem. Solids 6 (1958) 335.
[30] G.J. Small, J. Nucl. Mater. 125 (1984) 117.
[31] J.A. Turnbull, J. Nucl. Mater. 38 (1971) 203.
[32] R.S. Nelson, J. Nucl. Mater. 31 (1969) 153.
[33] R.M. Cornell, J. Nucl. Mater. 38 (1971) 319.
[34] A.D. Whapham, Nucl. Appl. 2 (1966) 123.
[35] R.M. Cornell, J.A. Turnbull, J. Nucl. Mater. 41 (1971) 87.
[36] J.A. Turnbull, R.M. Cornell, J. Nucl. Mater. 41 (1971) 156.
[37] W. Chubb, A.C. Hott, B.M. Argall, G.R. Kilp, Nucl. Tech. 26 (1975) 486.
[38] T.S. Noggle, J.O. Steigler, J. Appl. Phys. 31 (1960) 2199, in: R.J. White, M.O. Tucker, J. Nucl. Mater. 118 (1983) 1.
[39] C. Baker, J. Nucl. Mater. 66 (1977) 283.
[40] I.L.F. Ray, H. Thiele, Hj. Matzke, in: S.E. Donelly, J.H. Evans (Eds.), Fundamental Aspects of Inert Gases in Solids, Plenum, New York, 1991, p. 457.
[41] I.L.F. Ray, H. Thiele, Hj. Matzke, J. Nucl. Mater. 188 (1992) 90.
[42] S. Kashibe, K. Une, K. Nogita, J. Nucl. Mater. 206 (1993) 22.
[43] F. Sontheimer, P. Dewes, R. Manzel, H. Stehle, Proceedings of a Technical Committee Meeting, IAEA, Karlsruhe, 11–15 November 1985, IWGFPT/25, p. 108.
[44] C. Forat, B. Blanpain, B. Kapusta, P. Guedeney, P. Permezel, Proceedings of a Technical Committee Meeting, Pembroke, Ont., Canada, 28 April–1 May 1992, IAEA-TECDOC-697, p. 68.
[45] M. Lippens, Proceedings of an International Topical Meeting on LWR Fuel Performance, ANS/ENS, 21–24 April 1991, Avignon, France, p. 862.
[46] R. Manzel, R.P. Bodmer, G. Bart, Proceedings of a Technical Committee Meeting, Pembroke, Ont., Canada, 28 April–1 May 1992, IAEA-TECDOC-697, p. 63.
[47] R. Manzel, M. Coquerelle, M.R. Billaux, International Topical Meeting on Light Water Reactor Fuel Performance, West Palm Beach, FL, 17–21 April 1994, Proceedings, p. 335.
[48] M. Mogensen, C.T. Walker, I.L.F. Ray, M. Coquerelle, J. Nucl. Mater. 131 (1985) 162.
[49] T. Aoki, S. Koizumi, H. Umehara, K. Ogata, Proceedings of a Technical Committee Meeting, Pembroke, Ont., Canada, 28 April–1 May 1992, IAEA-TECDOC-697, p. 44.
[50] G.J. Small, ANS Topical Meeting on LWR Fuel Performance, April 17–20, 1988, Williamsburg, VA.
[51] R.J. White, ANS International Topical Meeting on Light Water Reactor Fuel Performance, April 17–21, 1994, West Palm Beach, FL.
[52] V.N. Chernikov, P.R. Kazansky, H. Trinkhaus, P. Jung, H. Ullmaier, in: S.E. Donelly, J.H. Evans (Eds.), Fundamental Aspects of Inert Gases in Solids, Plenum, New York, 1991, p. 329.
[53] V.F. Chkuaseli, Hj. Matzke, J. Nucl. Mater. 201 (1993) 92.
[54] R.J. White, International Topical Meeting on Light Water Reactor Fuel Performance, West Palm Beach, FL, 17–21 April 1994, Proceedings, p. 196.
[55] J.R. Matthews, G.J. Small, Proceedings of the conference on Water Reactor Fuel Element Computer Modelling in Steady State, Transient and Accident Conditions, Preston, UK, 18–22 Sept. 1988, p. 195, IWGFPT/32.
[56] D.A. MacInnes, I.R. Brearley, J. Nucl. Mater. 107 (1982) 123.
[57] R.J. White, paper presented in an IAEA Technical Committee Meeting on Nuclear Fuel Behaviour Modelling at High Burn-up and its Experimental Support, Windermere, UK, 19–23 June 2000.
[58] C. Ronchi, J. Nucl. Mater. 148 (1987) 316.
[59] L.E. Thomas, in: S.E. Donelly, J.H. Evans (Eds.), Fundamental Aspects of Inert Gases in Solids, Plenum, New York, 1991, p. 431.
[60] K. Nogita, K. Une, J. Nucl. Mater. 250 (1997) 244.
[61] D.R. Olander, Fundamental Aspects of Nuclear Reactor Fuel Elements. Report no. TID-26711-P1. Technical Information Centre, Office of Public Affairs, Energy Research and Development Administration, Oak Ridge, TN, 1976, p. 202.
[62] C. Ronchi, J. Nucl. Mater. 96 (1981) 314.
[63] H. Trinkhaus, in: S.E. Donelly, J.H. Evans (Eds.), Fundamental Aspects of Inert Gases in Solids, Plenum, New York, 1991, p. 369.
[64] D.M. Dowling, R.J. White, M.O. Tucker, J. Nucl. Mater. 110 (1982) 37.
[65] P. Lösönen, Nucl. Eng. Des. 196 (2000) 161.
[66] P. Lösönen, Nucl. Eng. Des. 201 (2000) 139.
[67] W.H. Press, S.A. Teukolsky, W.T. Vetterling, B.P. Flannery, Numerical Recipes in Fortran, 2nd Ed., Cambridge University, ISBN 0 521 43064 X, 1994, p. 702.
[68] I. Zacharie, S. Lansiart, P. Combette, M. Trotabas, M. Coster, M. Groos, J. Nucl. Mater. 255 (1998) 85.
[69] J.H. Evans, J. Nucl. Mater. 280 (1995) 302.